Journal of Experimental Botany, Vol. 73, No. 10 pp. 3283–3298, 2022
https://doi.org/10.1093/jxb/erab459 Advance Access Publication 17 October 2021
This paper is available online free of all access charges (see https://academic.oup.com/jxb/pages/openaccess for further details)

RESEARCH PAPER

Out of Africa: characterizing the natural variation in dynamic photosynthetic traits in a diverse population of African rice (*Oryza glaberrima*)

Sophie B. Cowling[1], Pracha Treeintong[1], John Ferguson[1,†], Hamidreza Soltani[2], Ranjan Swarup[1], Sean Mayes[1] and Erik H. Murchie[1,*]

[1] Division of Plant and Crop Science, School of Biosciences, University of Nottingham, Sutton Bonington Campus, Loughborough LE12 5RD, UK
[2] Advanced Data Analysis Centre, University of Nottingham, Sutton Bonington Campus, Loughborough LE12 5RD, UK

[†] Present address: Department of Plant Sciences, University of Cambridge, Cambridge CB2 3EA, UK.
* Correspondence: erik.murchie@nottingham.ac.uk

Received 6 September 2021; Editorial decision 14 October 2021; Accepted 15 October 2021

Editor: Tracy Lawson, University of Essex, UK

Abstract

African rice (*Oryza glaberrima)* has adapted to challenging environments and is a promising source of genetic variation. We analysed dynamics of photosynthesis and morphology in a reference set of 155 *O. glaberrima* accessions. Plants were grown in an agronomy glasshouse to late tillering stage. Photosynthesis induction from darkness and the decrease in low light was measured by gas exchange and chlorophyll fluorescence along with root and shoot biomass, stomatal density, and leaf area. Steady-state and kinetic responses were modelled. We describe extensive natural variation in *O. glaberrima* for steady-state, induction, and reduction responses of photosynthesis that has value for gene discovery and crop improvement. Principal component analyses indicated key clusters of plant biomass, kinetics of photosynthesis (CO_2 assimilation, *A*), and photoprotection induction and reduction (measured by non-photochemical quenching, NPQ), consistent with diverse adaptation. Accessions also clustered according to countries with differing water availability, stomatal conductance (g_s), *A*, and NPQ, indicating that dynamic photosynthesis has adaptive value in *O. glaberrima*. Kinetics of NPQ, *A*, and g_s showed high correlation with biomass and leaf area. We conclude that dynamic photosynthetic traits and NPQ are important within *O. glaberrima*, and we highlight NPQ kinetics and NPQ under low light.

Keywords: African rice, dynamic modelling, natural variation, NPQ, *O. glaberrima*, photosynthesis, rice, stomatal conductance.

Introduction

The climate crisis places crop yields under increasing pressure from biotic and abiotic constraints and constitutes a major threat in meeting global food demand (Ray *et al.*, 2019). Substantial yield decreases in key cereal crops are predicted to occur in both vulnerable and productive regions (Black *et al.*, 2008; Challinor *et al.*, 2014). Asian rice (*Oryza sativa*), a dietary

stable to a third of the global population, is predicted to experience yield losses up to 37% by the end of the century due to climate change-driven drought events Bocco *et al.*, 2012; Zhao *et al.*, 2017). The development of productive and resilient rice cultivars has been the subject of increasing research focus (Atwell *et al.*, 2014), and advances have been made through traditional plant breeding methods within the *O. sativa indica* and *japonica* types. However, there has also been an interest in the introgression of genes from a range of diverse interspecific material. This includes the African rice species *Oryza glaberrima*, which was domesticated in Africa 2000–3000 years ago, independently of the domestication of Asian rice *O. sativa*. *Oryza glaberrima* retains many properties that are specific to challenging African conditions of soil and climate, including limited water availability, abiotic stress, pests, and diseases (Bimpong *et al.*, 2011; Agnoun *et al.*, 2012; Bocco *et al.*, 2012; Cubry *et al.*, 2020).

Oryza glaberrima is not suitable for commercial rice production due to lodging, shattering, milling difficulties, and low yields in comparison with *O. sativa* (Linares, 2002). However, the resilience to a range of abiotic and biotic stresses makes *O. glaberrima* an attractive target for gene mining and translation (Fig. 1; Sarla and Swamy, 2005), which was one of the motivations for the interspecific New Rice for Africa (NERICA) breeding programme (Wambugu *et al.*, 2019). This underlying genetic diversity might allow commercial rice to tolerate increasingly unpredictable climatic conditions. Recent genomic sequencing advances for *O. glaberrima* have now added new possibilities (Cubry *et al.*, 2020).

Photosynthetic efficiency and water use efficiency (WUE) are important components of productivity and abiotic stress resilience (Zhao *et al.*, 2017). Stomata are key players in both processes, regulating CO_2 assimilation (A; the parameter abbreviation list can be found in Supplementary Table S1 and the water lost by transpiration via stomatal conductance (g_s). However, improvements in WUE incorporate a trade-off between transpiration rate at the expense of net CO_2 assimilation rate (A) (Blum, 2009; Lawson *et al.*, 2010; Lawson and Blatt, 2014). The leaf stomatal density (SD) value can affect g_s; recent work using rice with reduced SD has demonstrated that photosynthesis was not compromised in well-watered conditions but enhanced WUE in all conditions and improved biomass and yield under water limitation (Caine *et al.*, 2019; Mohammed *et al.*, 2019). Consequently, improved yield in water-limiting environments might be achieved by optimization of stomatal morphology and density. Dynamics of stomatal aperture alteration have also been increasingly highlighted as playing an essential role in improving photosynthetic efficiency and WUE (Drake *et al.*, 2013; Lawson and Blatt, 2014). Stomata can take some time to reach stable g_s (McAusland *et al.*, 2016). Increasing the speed of stomatal opening and closing, closely coupling to A (Fig. 1), may be important in conserving water and improving crop yields (Lawson and Vialet-Chabrand, 2019).

Historically, light-saturated carbon assimilation capacity (A_{max}) (mostly under ambient atmospheric [CO_2]) has been a parameter of interest for photosynthesis improvements (Murchie *et al.*, 2018). However, recent research now makes it clear that the dynamic responses of photosynthesis and photoprotection [such as non-photochemical quenching (NPQ)] to the fluctuating field environment are essential for photosynthetic efficiency-based yield gains (Kromdijk *et al.*, 2016; Taylor and Long, 2017; Murchie *et al.*, 2018; Acevedo-Siaca *et al.*, 2020). Light in plant canopies is transient due to architecture, intermittent cloud cover, solar angle, and wind (Burgess *et al.*, 2016). The ability of A to rapidly adjust to changes in light levels is limited by two major processes: stomatal dynamics and photosynthetic biochemistry (McAusland

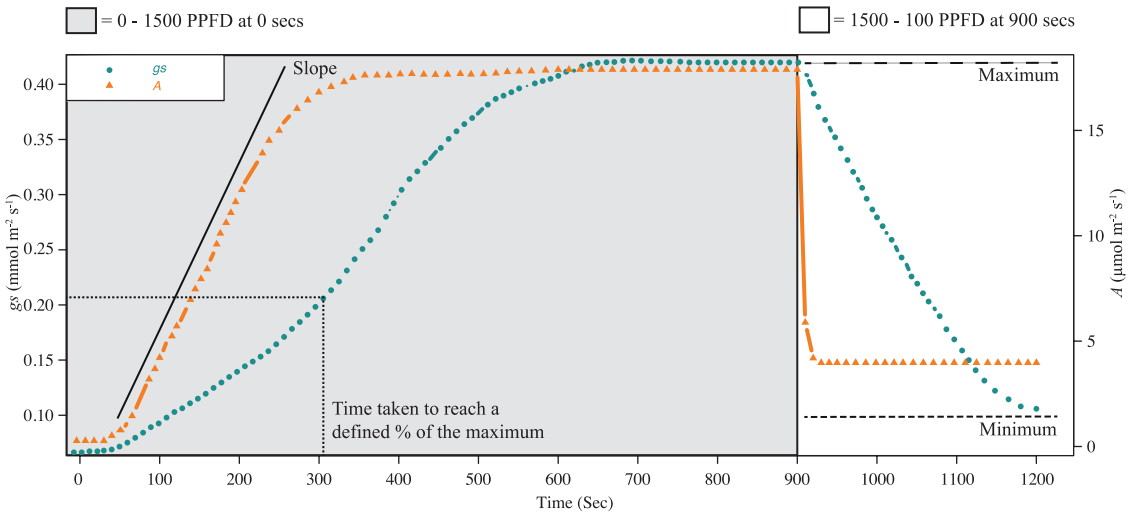

Fig. 1. Schematic showing example induction and reduction in response to changes in light intensity during gas exchange measurements. These examples of raw A and g_s gas exchange measurements show the modelled dynamic response parameters; minimum, maximum, slope, and time to reach a defined percentage of the curve maximum.

et al., 2016; Slattery *et al.*, 2018; Acevedo-Siaca *et al.*, 2020). In wheat, slow induction dynamics were estimated to cost 21% of carbon assimilation acquisition (Taylor and Long, 2017). Further dynamic leaf photosynthetic efficiency can be improved through the rapid relaxation of photoprotection (Kromdijk *et al.*, 2016; Hubbart *et al.*, 2018). Under high light, NPQ dissipates excess excitation energy as heat. However, in fluctuating light conditions, NPQ dynamics can lag behind shifts in light level, limiting photosynthesis. On this basis, it is clear that elucidating photosynthesis-related dynamics is an essential focus of improving crop yields and improving abiotic stress tolerance, whereby plants can utilize light and CO_2 with increased efficiency.

Variation in photosynthetic, NPQ, and stomatal traits have been examined in *O. sativa*; however, there is no comprehensive analysis which compares both induction and decline. We hypothesize that due to the origins within the diverse African climates, substantial variation for dynamic photosynthesis traits may exist within the genome of *O. glaberrima* and we have used a new, whole-genome re-sequenced, resource of 155 *O. glaberrima* accessions (Wambugu *et al.*, 2019; Cubry *et al.*, 2020) to characterize 58 phenotypic traits for photosynthesis and leaf WUE. This includes the use of automated machine learning to describe SD and gas exchange methods to facilitate the modelling of *A*, NPQ, and g_s induction and decline dynamics across a large population of individuals. Furthermore, as the effect of environment-driven trait adaptation is central to the novelty of *O. glaberrima*, we explore the effect of 20 climatic variables and ecotype upon trait adaptation within the population. Here, we describe an African rice population with broad heritable variation in a range of useful traits and we provide evidence that dynamic and steady-state photosynthesis and photoprotective traits are linked to whole-plant growth. To our knowledge, this is the largest survey of dynamic photosynthesis for a species in the *Oryza* genus to date. This further highlights the importance of *O. glaberrima* as an essential source of variation for crop improvement and providing a solid base for future research to elucidate physiological processes and pursue trait-related gene identification.

Materials and methods

Plant material and growth conditions

The seeds of 155 *O. glaberrima* accessions were provided by the Interspecies Comparison & Evolution (RICE) team within Diversité Adaptation Developpement des plantes (DIADE), IRD-Montpellier, France. A table of information presenting the plant material is provided in Supplementary Table S2.

Plants were grown, measured, and processed at the Sutton Bonington Campus, University of Nottingham, UK. Plants were sown and grown in a controlled-environment agronomy-style glasshouse (Cambridge HOK, UK). Conditions were maintained at a 12 h dark:light (07.00–19.00 h) photoperiod, controlled using blackout blinds, temperature of 28±3 °C, and 50–60% relative humidity. Metal halide lamps were used to maintain light levels when they fell below 200 μmol m^{-2} s^{-1} photosynthetically active radiation (PAR). Seeds were heat treated to prevent pathogenesis at the primary seedling stage through immersing in water at 55 °C for 15 min. Seeds were germinated in a module tray for 2 weeks before being transplanted to soil pits (5 m×5 m×1.25 m, L×W×D) within the glasshouse. Five replicates of each accession were transplanted in east–west rows, at 20 cm intervals, into high nutrient loam-based soil in 2×5 m concrete pits. Plants were irrigated by drip tapes twice a day, to provide a soil water content close to field capacity. Soil top layers were replaced every 2 weeks from the same batch.

Due to the size of the population accessions, planting was staggered at 1–2 week intervals. Accessions were grown in rotations of 12 genotypes at a time, with five biological replicates, four of which were selected for measurement. Plants were measured at 8 weeks old when they were approximately in the mid to late tillering stage. Measurements commenced in July 2017 and ended in October 2017. The elite *O. sativa* variety 'IR64' was used as a reference genotype and planted as a row in every batch (see 'Data analysis' below).

Gas exchange measurements

An IRGA (infra-red gas analyser; Li-Cor 6400XT, Lincoln, NE, USA) was used on the uppermost fully expanded leaf. A light induction programme was used: leaves were dark adapted for 1 h, the sample leaf was then placed in the leaf cuvette and allowed to achieve steady state in darkness before being subject to a photosynthetic photon flux density (PPFD) of 1500 μmol m^{-2} s^{-1}, from in-built red and (10%) blue LED lights, from 0 s to 900 s, reducing to 100 μmol m^{-2} s^{-1} from 900 s to 1200 s. A graphical representation of the induction assay can be seen in Fig. 1. The leaf cuvette conditions were maintained at a block temperature of 30 °C, 400 μmol^{-1} mol^{-1} CO_2, flow rate 500 ml min^{-1}, and 50–65% humidity. Gas exchange data were logged every 10 s. Measurements were collected between 09.00 h and 16.00 h. Chlorophyll fluorescence parameters were collected simultaneously, by applying a single saturating pulse before the application of actinic light to attain F_o and F_m and then at intervals of 60 s following this for the calculation of ϕPSII (PSII operating efficiency in the light), qP (photochemical quenching), and NPQ (non-photochemical quenching: measurement of a photoprotective process that estimates the rate constant for PSII heat loss) (Murchie and Lawson, 2013). Intrinsic water use efficiency (iWUE) was calculated post-data collection as CO_2 assimilation rate (*A*)/stomatal conductance (*gs*). We calculate that vapour pressure deficit (VPD) in the cuvette was ~1.51–2.10 kPa. Saturation or near-saturation was achieved within this time scale. Raw data for *A*, g_s, and NPQ are shown graphically in Supplementary Fig. S1 as individual replicates and means per accession.

Stomatal density and automated stomatal counting

Stomatal impressions were taken from the same area of the first fully expanded leaf where the IRGA measurements were obtained. A ~1 cm^2 negative impression of the abaxial (basal) and adaxial (upper) leaf surface was taken using fast-drying clear nail polish and adhered to a microscope slide. Impressions were obtained after all other measurements had been taken.

Images were obtained on a Leica DM5000B light microscope at ×40 objective with 10 fields of view per impression. Due to the volume of images (13 110), a bespoke machine learning-based software was created to automatically calculate the number of stomata in each image. The software can reliably identify *O. glaberrima* and *O. sativa* stomata, showing a high correlation (r=0.94; n=540 images per counting method) between software and manual stomatal counts. Our method was based on transfer learning for deep neural networks: we have utilized a pre-trained deep model for the different datasets and adapt it for user-annotated rice stomata samples. Based on the transfer learning approach, we utilize a pre-trained object detection model trained on the

standard COCO datasets (Lin *et al.*, 2014). Since our goal is detecting and classifying stomata, we use the Faster R-CNN model (Ren *et al.*, 2015) as one of the state-of-the-art methods based on deep neural networks. We used the Faster R-CNN model available in Tensorflow with the Inception-V2 architecture (Szegedy *et al.*, 2016) as the base model. Inception-V2 is a variation of Inception-V1, also referred to as GoogLeNet, which was the state-of-the-art architecture at the ImageNet competition in ILSVRC 2014. After loading the pre-trained Faster R-CNN, the last few layers of classification layers are changed to meet the aim of stomata classification and detection. In the next step, the Faster R-CNN with stomata images are trained with different hyperparameters such as learning rate and number of epochs to find out the best parameters to reduce execution time and errors. Further information on our methodology is located in File S1 at the Zenodo repository https://doi.org/10.5281/zenodo.5555930; Murchie, 2021).

Morphological traits

Plant height, leaf area, and root and shoot dry biomass were taken at 8 weeks post-germination, after the completion of gas exchange measurements. Each plant was dug up and care taken to preserve the root system. The shoot area was measured using a LiCor LI-3100 area meter. The root ball was soaked and carefully washed to preserve root structure, as described by York (2018). The shoot and root material were then placed in a drying oven at 70 °C for 72 h before weighing for dry biomass.

Data analysis

All data analyses were performed using R-Studio (v. 4.0.1).

To reduce the temporal and spatial effects of measuring the accessions in batches, a linear mixed-effects model ('lme4' package, v.1.1-26) was used to calculate best linear unbiased predictions (BLUPs) and predicted means, considering the effects of accession, sowing date, measurement date, location within the glasshouse, and, if relevant, IRGA machine (Supplementary Fig. S2). BLUPs are commonly used to account for the random effects that accompany measuring large populations in fluctuating environments (Robinson, 1991; Merk *et al.*, 2012). The coefficients of the mixed-effects model were also used to estimate broad sense heritability (H^2). All results reported here use the adjusted means data generated from the mixed-effects model. Normality was tested using the Shapiro–Wilk test. A 0.01 α value was used, as the Shapiro–Wilk test tends to report false negatives in sample sizes exceeding 50 individuals. All data for IR64 were found to be normally distributed, whereas 25 out of 57 traits in the *O. glaberrima* panel showed a deviation from a statistically normal distribution. In the results, and *O. glaberrima* descriptive statistics Table 1, non-normal traits report values for median and interquartile range (IQR), whereas normally distributed traits will report mean and standard deviation. A full breakdown of IR64 and *O. glaberrima* normality statistics, box, and distribution plots can be found in Files S2–S4 at Zenodo.

A bespoke Python pipeline was written to identify the data point at 95% of the maximum and extract values within the induction side of a curve (File S5 at Zenodo).

The correlation analyses were completed using a Pearson correlation coefficient in the 'Corrplot' package (v. 0.84), with a correlation significance threshold of $P<0.1005$.

The percentage genetic variation (PGV) was calculated as follows; $[(x_{max}–x_{min})/x)]\times100$. Where x_{max}, x_{min}, and x, respectively, denote the maximum, minimum, and mean values for a trait in the population (Gu *et al.*, 2014). This measure is used to quantify the genetic variation of a trait within the combined population. Values >100% signify where the range is greater than the mean and represent particularly high underlying genetic variation.

Kinetic modelling

Dynamic modelling of A, NPQ, and g_s was performed using a dose–response curve-fitting method, previously used to model stomatal responses by Barratt *et al.* (2021). The 'drc' (v. 3.0) package was used to analyse and extract several useful parameters for both curve induction and reduction responses (Ritz *et al.*, 2015), denoted by $_i$ and $_r$, respectively. The measured parameters are detailed in Table 1 and include curve slope ($_{i/r\ slope}$), lower limit ($_{i/r\ min}$), upper limit ($_{i/r\ max}$), and the time taken to reach a defined percentage of the dependent variable, in this case 10 ($_{i/r\ 10}$), 50 ($_{i/r\ 50}$), and 90% ($_{i/r\ 90}$). A representation of these parameters on A and g_s response curves can be found in Fig. 1. The LL.4 (log-logistic 4-parameter) model was chosen as the best fit for both the A induction, and g_s induction and reduction responses. The LL.3 (log-logistic 3-parameter) model was used for NPQ induction, and the W2.4 (4-parameter Weibull2) model for NPQ relaxation. The comparison of eight different models, followed by Akaike's information criterion analysis, was used to select the best model fit. All 155 accessions were analysed for A induction curves; 24 accessions were removed for g_s induction and g_s reduction curve fitting due to unusable curve measurements.

Due to the volume of data, the best fitting model was selected for the induction and reduction curve for each parameter (g_s, A, and NPQ) and then applied to all data (e.g. for g_s induction, a LL.4 model was applied to all 155 genotypes). To ensure that the model selection process captured the variation that may occur in the population, five genotypes were randomly chosen for model selection and the consensus model was used. The estimated parameters generated from the model (min, max, ed50, and slope) were manually cross-referenced to the raw data, to ensure these outputs closely represented the raw data. To evidence the fit of the selected models to the raw data, we include a table showing the model fit of a randomly selected accession for each parameter (Supplementary Table S3). We note the large SE for $A_{r\ slope}$, probably due to the rapid and steep drop in A that occurs between two data points, so we attribute less confidence in this parameter.

Multivariate and climatic analysis

The multivariate analyses, principal component analysis (PCA), and hierarchical clustering (H-clustering) methods require a complete dataset, with no missing values. Consequently, missing phenotype data were imputed using the missMDA package (v. 1.18). PCA was performed using the FactoMineR (v. 2.4) package, and the H-clustering was performed using the HCPC method. Details of the FactoMineR package and HCPC algorithm can be found in Lê *et al.* (2008).

The PCA and H-clustering of the phenotypic dataset contained all 155 *O. glaberrima* accessions and the IR64 *O. sativa* representative. The analysis included 64 quantitative trait variables and four qualitative variables, namely narrow ecotype, broad ecotype, country of origin, and African region.

Agroecological niche and geographical coordinates of the collection sites for each *O. glaberrima* accession were provided by AfricaRice. We have complete ecological information for all 155 accessions, and geographical coordinates for 105 accessions (Fig. 2A–C). Nineteen variables for temperature and precipitation, at the collection site of each accession, were obtained using the BIOCLIM dataset (Hijmans *et al.*, 2005). Information on the elevation above sea level was obtained using the elevatr package (v. 0.3.1). PCA and H-clustering analysis, and subsequent climate–trait correlations, were performed on the subset of 105 accessions for which we had geographical coordinates.

Table 1. The range of natural variation and broad-sense heritability (H^2) within a population of diverse *O. glaberrima* accessions across dynamic and static traits

Trait	Min	Max	Mean (SD)	Median (IQR)	PGV	Sig.	H^2
Steady state							
A_{max}	17.92	22.42	20.16 (0.87)		22.30	***	0.11
ETR_{max}	104.10	144.30	123.00 (7.60)		32.69	***	0.22
g_{smax}	0.26	0.46	0.34 (0.03)		58.82	***	0.17
$iWUE_{max}$	58.34	71.81		62.63 (3.08)	21.40	***	0.07
NPQ_{max}	1.98	2.30	2.13 (0.06)		14.88	***	0.12
$\phi PSII_{max}$	0.16	0.22	0.19 (0.01)		32.70	***	0.22
qP_{max}	0.43	0.51	0.47 (0.02)		18.71	***	0.17
$Trmmol_{max}$	4.13	5.75	4.81 (0.27)		29.84	***	0.12
VPD_{max}	1.43	1.52	1.47 (0.01)		6.38	***	0.00
Morphological							
Shoot:root	3.36	9.50		5.55 (1.13)	73.22	***	0.12
Shoot biomass	2.36	7.85		4.40 (0.89)	123.33	***	0.14
Shoot area	279.07	1068.97		652.73 (126.27)	118.51	***	0.16
Root biomass	0.36	1.98		0.77 (0.18)	203.75	***	0.23
Plant height	61.79	93.86	78.77 (6.20)		40.72	***	0.18
Adaxial SD	260.16	353.50	314.08 (18.04)		29.72	***	0.21
Abaxial:adaxial	1.05	1.40	1.24 (0.06)		18.87	***	0.15
Abaxial SD	324.31	435.99	388.83 (22.54)		28.72	***	0.21
Dynamic							
$g_{si\ slope}$	–3.90	–1.90		–2.44 (0.38)	78.43	***	0.14
$g_{si\ max}$	0.35	0.49	0.42 (0.03)		31.88	*	0.11
$g_{si\ min}$	0.06	0.14		0.08 (0.01)	112.50	**	0.12
$g_{si\ 10}$	65.50	207.09		108.19 (29.45)	126.83	***	0.18
$g_{si\ 50}$	179.53	324.80		223.71 (48.40)	64.17	*	0.11
$g_{si\ 90}$	477.70	684.41		539.21 (48.40)	37.53	NS	0.08
$g_{si\ rate}$	0.0005	0.0008		0.0006 (<0.01)	45.45	*	0.09
$A_{i\ slope}$	–2.42	–1.50		–1.78 (0.17)	50.84	**	0.10
$A_{i\ max}$	20.44	27.83	23.43 (1.47)		31.53	***	0.20
$A_{i\ min}$	–1.32	–1.09	–1.22 (0.04)		18.85	NS	0.01
$A_{i\ 10}$	49.01	140.97		63.79 (13.96)	136.43	***	0.15
$A_{i\ 50}$	189.56	334.26		217.84 (24.73)	64.97	**	0.12
$A_{i\ 90}$	652.34	849.54		718.78 (52.10)	27.14	NS	0.06
$A_{i\ rate}$	0.03	0.04	0.03 (0.002)		33.33	NS	0.05
$NPQ_{i\ slope}$	–3.48	–2.32		–2.72 (0.22)	42.65	***	0.12
$NPQ_{i\ max}$	2.12	2.44	2.24 (0.05)		14.29	***	0.08
$NPQ_{i\ 10}$	19.57	28.12	23.80 (1.53)		35.75	***	0.11
$NPQ_{i\ 50}$	50.98	56.44	53.65 (1.02)		10.16	NS	0.05
$NPQ_{i\ 90}$	118.70	132.30	125.58 (2.71)		10.82	NS	0.03
$NPQ_{i\ rate}$	0.017	0.02	0.02 (<0.01)		15.00	**	0.07
$g_{sr\ slope}$	6.48	10.49		8.05 (0.80)	49.43	NS	0.07
$g_{sr\ min}$	-0.30	0.02		-0.13 (0.08)	228.57	**	0.11
$g_{sr\ max}$	0.38	0.61	0.48 (0.05)		48.96	**	0.15
$g_{sr\ 10}$	908.91	956.10		922.35 (8.56)	05.11	NS	0.07
$g_{sr\ 50}$	1061.65	1385.05	1208.21 (76.16)		26.77	***	0.26
$g_{sr\ 90}$	1370.52	2116.04		1640.46 (266.31)	44.56	***	0.23
$g_{sr\ rate}$	0.0006	0.0101		0.001 (<0.01)	339.28	***	0.25
$A_{r\ slope}$	-332.60	-322.20		-328.45 (2.15)	3.17	NS	0.01
$A_{r\ min}$	2.88	3.60	3.22 (0.11)		24.05	***	0.11
$A_{r\ max}$	17.09	21.72	19.22 (0.96)		22.36	NS	0.04
$A_{r\ 10}$	901.90	902.20	902.09 (0.04)		0.03	NS	0.03
$A_{r\ 50}$	905.30	905.70		905.45 (0.05)	0.04	NS	0.03
$A_{r\ 90}$	910.60	911.00		910.77 (0.05)	0.04	NS	0.02
$A_{r\ rate}$	0.79	2.36		1.51 (0.09)	103.97	*	0.08

Table 1. Continued

Trait	Min	Max	Mean (SD)	Median (IQR)	PGV	Sig.	H^2
$NPQ_{r\ slope}$	–49.71	–36.27	–41.83 (2.65)		34.35	***	0.21
$NPQ_{r\ min}$	0.56	0.66	0.61 (0.02)		23.00	***	0.16
$NPQ_{r\ max}$	1.99	2.30	2.13 (0.06)		14.55	***	0.10
$NPQ_{r\ 10}$	921.31	923.66	922.60 (0.39)		0.27	***	0.19
$NPQ_{r\ 50}$	946.63	954.76	950.23 (1.41)		0.97	***	0.19
$NPQ_{r\ 90}$	985.20	1008.16	995.50 (4.13)		02.50	***	0.19
$NPQ_{r\ rate}$	0.013	0.020	0.016 (<0.01)		43.75	***	0.14

Normally distributed traits report the trait mean and standard deviation, whilst the median and interquartile range is given for non-normally distributed traits. PGV is the percentage of genetic variation. Sig. refers to the ANOVA test between two mixed-effects models, where the accession is present as an effect in one model and not in another. A significant result suggests that the accession genotype has an effect and therefore the trait is heritable. ***P<0.0001, **P<0.001, *P<0.01

FactoShiny was used to generate summary reports of the PCA and H-clustering analyses on both the phenotype data and climate data; these can be found in Files S6–S9 at Zenodo.

Results

Phenotypic analysis of morphology and steady-state photosynthesis

Significant variation and high levels of PGV were identified between accessions across all morphological, gas exchange, and fluorescence traits measured in this *O. glaberrima* panel (Table 1; Files S2, S4 at Zenodo).

Root biomass, shoot biomass, and shoot area showed a 5-, 3-, and 4-fold variation, respectively. Plant height showed a 1.3-fold variation in PGV. Significant (P<0.001) positive correlations between all plant growth traits were found (Fig. 3A, C).

Even though key steady-state photosynthesis traits showed a relatively narrow distribution (typically between 15% and 40%), both shoot biomass and shoot area showed significant (P<0.01–0.05; Fig. 3A; File S10 at Zenodo), positive correlations to A_{max}, qP_{max}, ETR_{max}, and $\phi PSII_{max}$, providing confidence that steady-state photosynthesis is linked to biomass production. g_{smax} showed an almost 2-fold variation across *O. glaberrima* accessions. PGV for steady-state traits ranged from 6.38% to 58.82% (Table 1), with most traits in the 20–30% range, including key photosynthetic traits. All key steady-state photosynthetic traits showed significant (P<0.0001) positive correlations to one another (Fig. S3). Some unexpected relationships were apparent, for example between NPQ_{max} and VPD_{max}. $iWUE_{max}$ was highly correlated with g_{smax} (Fig. 3B) (and $Trmmol_{max}$) but not A_{max}, indicating stomatal limitation of A.

Stomatal morphology (Fig. 4) did not show a clear relationship with conductance. A relatively modest 1.3-fold accession-dependent variation in the abaxial SD and adaxial SD was observed. The abaxial SD was 1.24-fold greater than the adaxial SD. PGV showed that all SD traits were highly significant (P<0.0001, Table 1) across the *O. glaberrima* accessions, revealing that SD has a genetic basis. However, no association between any SD traits and $iWUE_{max}$, or g_{smax} was detected. Unexpectedly the adaxial SD showed a significant negative correlation to NPQ_{max}, while abaxial SD showed a negative association with plant height (Fig. 3D). The SD ratio, however, showed significant associations with multiple traits (Fig. 3C); A_{max}, ETR_{max}, $\phi PSII_{max}$, qP_{max}, NPQ_{max}, and plant height, the reasons for which are unclear.

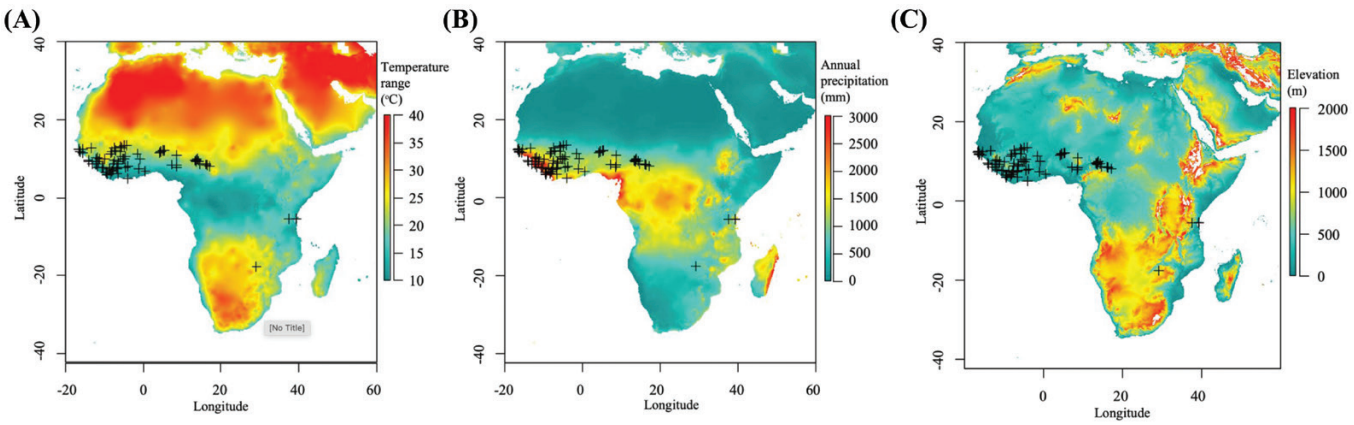

Fig. 2. Map showing the geographical collection locations of *O. glaberrima* accessions used in this study. The annual range of (A) temperature, (B) annual precipitation, and (C) elevation across Africa.

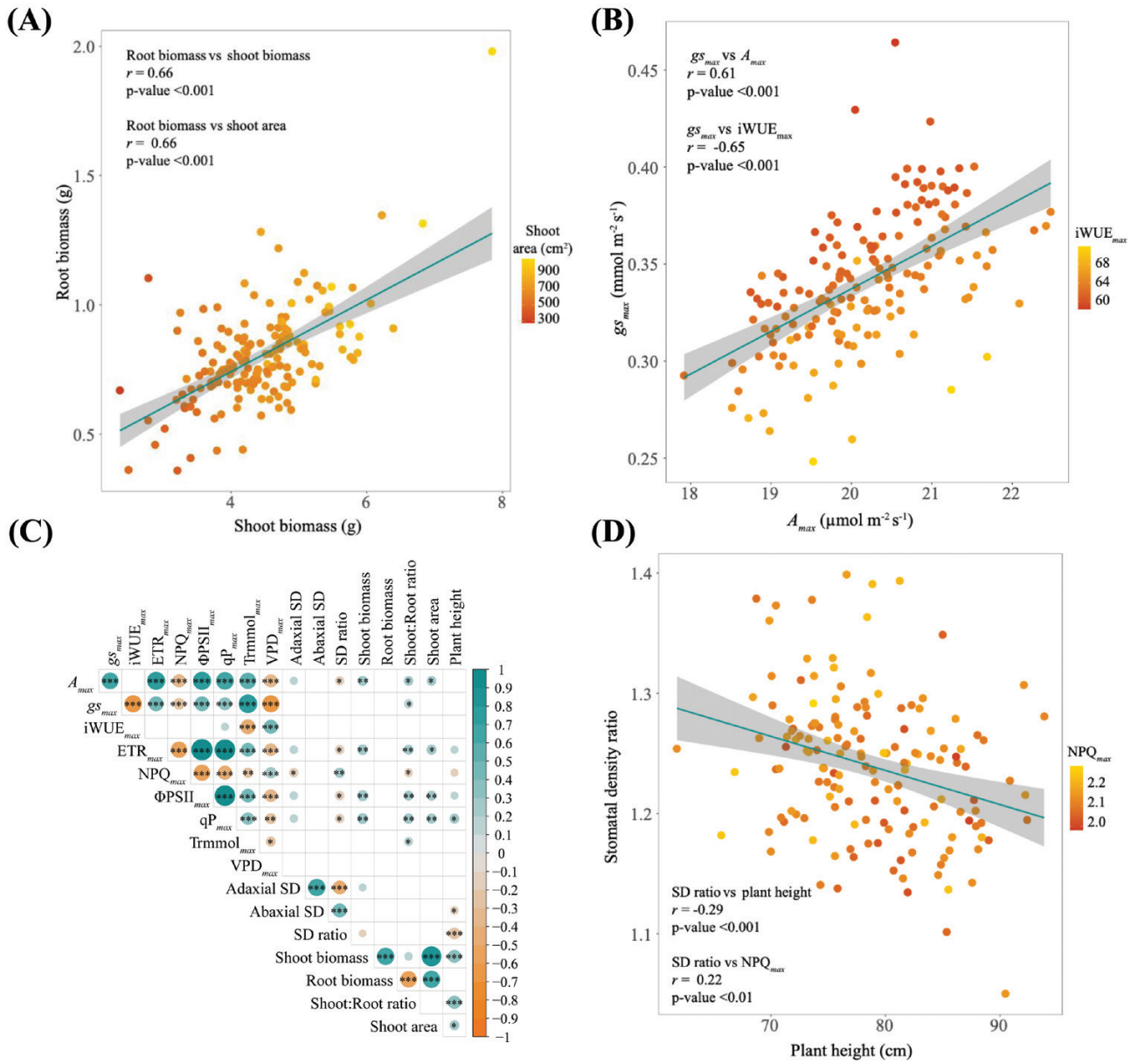

Fig. 3. *O. glaberrima* shows a range of interesting morphological and steady-state photosynthetic trait correlations. The colour gradient shows a second correlation against the *y*-axis variable. (A) Positive correlation between root and shoot biomass; the second correlation shows root biomass and shoot area. (B) The effect of g_{smax} on A_{max} and the second correlation of g_{smax} against $iWUE_{max}$. (C) Pearson correlation matrix showing associations between morphological and steady-state gas exchange traits, filtered to show trait associations at a $P<0.1005$ significance threshold. Correlations are scaled by colour, shown in the right-hand scale bar; asterisks indicate significance between traits (***$P<0.001$, **$P<0.01$, *$P<0.05$). (D) Negative correlation between SD ratio and plant height, while the SD ratio against NPQ_{max} shows a positive correlation.

Phenotypic analysis of dynamic photosynthesis

Dynamic responses are now recognized as important determinants of photosynthetic productivity. Responses of gas exchange, fluorescence, and photoprotection to light shifts were modelled and show significant variation in 29 traits (Table 1, column 'Sig'; Figs 5A–D, 6A, B; Supplementary Fig. S4A–F).

The well-documented divergence between the induction of g_s and A was observed, where a lag in g_s induction and reduction occurs relative to A (Figs 1, 5A–C). The mean upper limit estimates for A induction and reduction curves ($A_{i\ max}$ and $A_{r\ max}$) and g_s induction and reduction ($g_{sr\ max}$ and $g_{si\ max}$) curves were similar ($P<0.0001$, Supplementary Fig. S5A, B) to measured values. The estimated averages for the mean lower limits of the A induction ($A_{i\ min}$), g_s induction and reduction ($g_{si\ min}$ and $g_{sr\ min}$) curves are close to zero (Table 1).

The average time taken to reach 10% of the maximum induction curve was significantly less for CO_2 assimilation ($A_{i\ 10}$) than for g_s ($g_{si\ 10}$), whereas the time taken to reach 50% of the

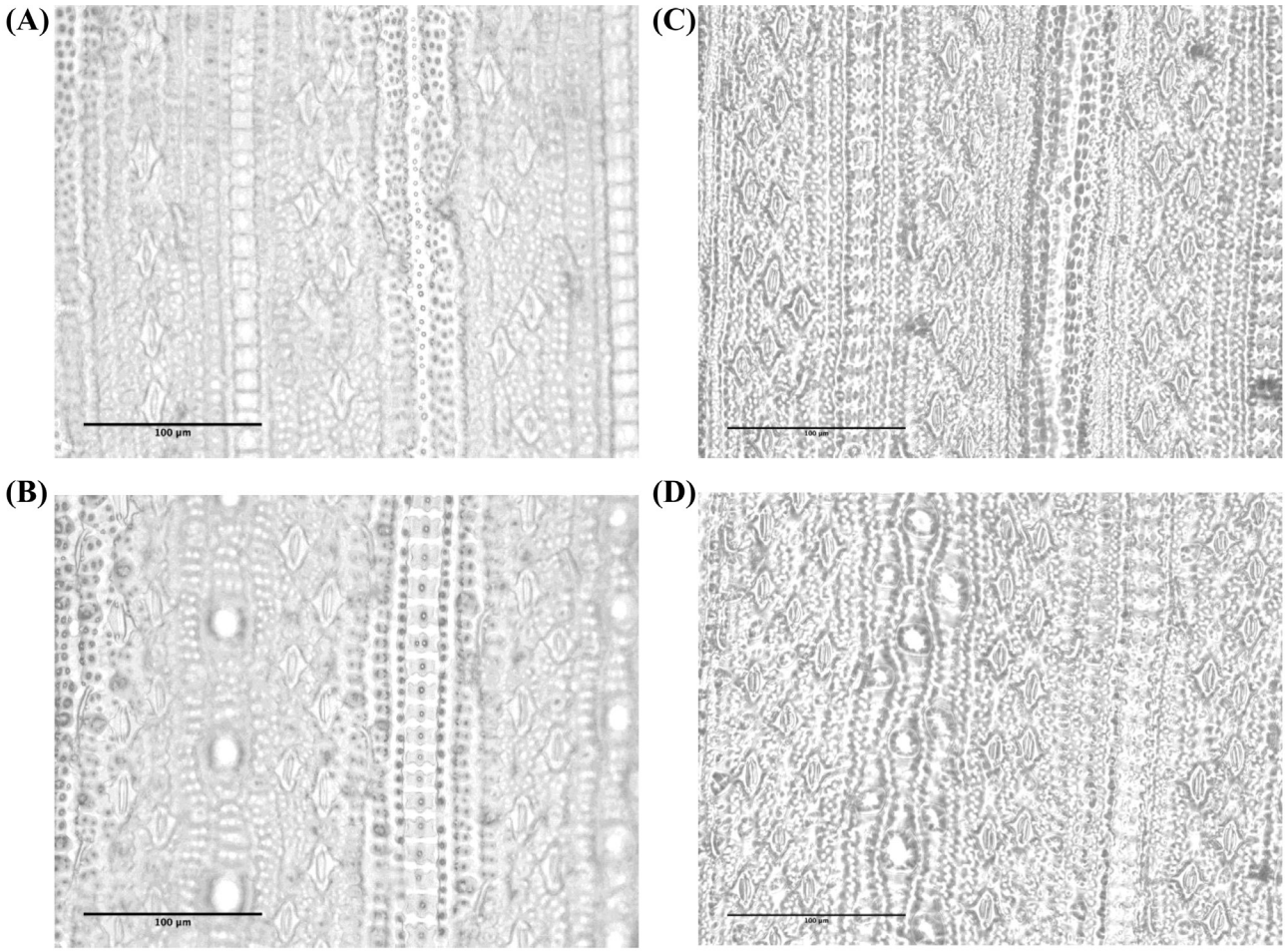

Fig. 4. Microscope images showing examples of the *O. glaberrima* accessions with highest (TOG_14116) and lowest (TOG_5464) recorded SD. These images demonstrate the extent of SD variation in the population and the qualitative correlation between high SD and small stomatal size, (A) TOG_5464; adaxial SD=260 mm^{-2}, (B) TOG_5464; abaxial SD=325 mm^{-2}, (C) TOG_14116; adaxial SD=345 mm^{-2}, (D) TOG_14116; abaxial SD=426 mm^{-2}.

induction curve for $A_{i\ 50}$ and $g_{si\ 50}$ did not significantly differ. However, the average time to reach induction to 90% of the maximum ($A_{i\ 90}$) was significantly longer than that of $g_{si\ 90}$.

Strong interactions between stomatal and CO_2 assimilation indicate co-dependence (Fig. 5E, F). Notably the steepness of the g_s induction slope ($g_{si\ slope}$) highly correlates with key induction traits $g_{si\ 90}$, $g_{si\ rate}$, g_{smax}, $A_{i\ slope}$, $A_{i\ rate}$, $_iWUE_{max}$, NPQ_{islope}, NPQ_{imax}, and NPQ_{i50}. $g_{si\ rate}$ was also strongly correlated to many dynamic induction traits; g_{smax}, $g_{si\ 10}$, $g_{si\ 50}$, $g_{si\ 90}$, A_{max}, $A_{i\ 90}$, and $A_{i\ rate}$.

The rate of photosynthetic induction in high light was associated with rates of decline in low light (Fig. 5). $g_{si\ slope}$ versus $g_{sr\ slope}$, $gs_{i\ rate}$ versus $gs_{r\ rate}$, and $A_{i\ rate}$ versus $A_{r\ rate}$ were significant, suggesting that accessions which exhibited rapid stomatal opening also close at a greater rate (Fig. 5C, D; Supplementary Fig. S5). Further, traits associated with rapid stomatal closure, $g_{sr\ slope}$, $g_{sr\ 10}$, $gs_{r\ 50}$, and $g_{sr\ 90}$ showed significant associations with enhanced $iWUE_{max}$.

Like steady-state traits, A and g_s dynamics were also linked to plant biomass and morphology in these data, further supporting the role of photosynthesis in determining growth. A greater $A_{i\ rate}$ was positively correlated with total plant and shoot biomass. $A_{r\ rate}$ showed positive associations with total plant biomass, shoot biomass, shoot:root ratio, and shoot area. $A_{r\ slope}$ had negative associations with shoot biomass, shoot:root ratio, and plant height, while a more rapid $A_{r\ 90}$ was correlated to a greater shoot biomass, shoot:root ratio, and shoot area. $g_{si\ rate}$ showed positive associations with total plant biomass, shoot biomass, root biomass, and shoot area.

Again there were fewer links with stomatal morphology; a significant negative association was identified between the SD ratio and $A_{r\ rate}$. Only upper leaf SD was also found to have positive relationships to $g_{si\ 50}$ and $A_{r\ rate}$, and a negative relationship to $g_{sr\ min}$.

Non-photochemical quenching dynamics

NPQ is of particular interest here because it showed multiple relationships with photosynthesis and biomass. The model estimation of the NPQ induction and relaxation curve upper

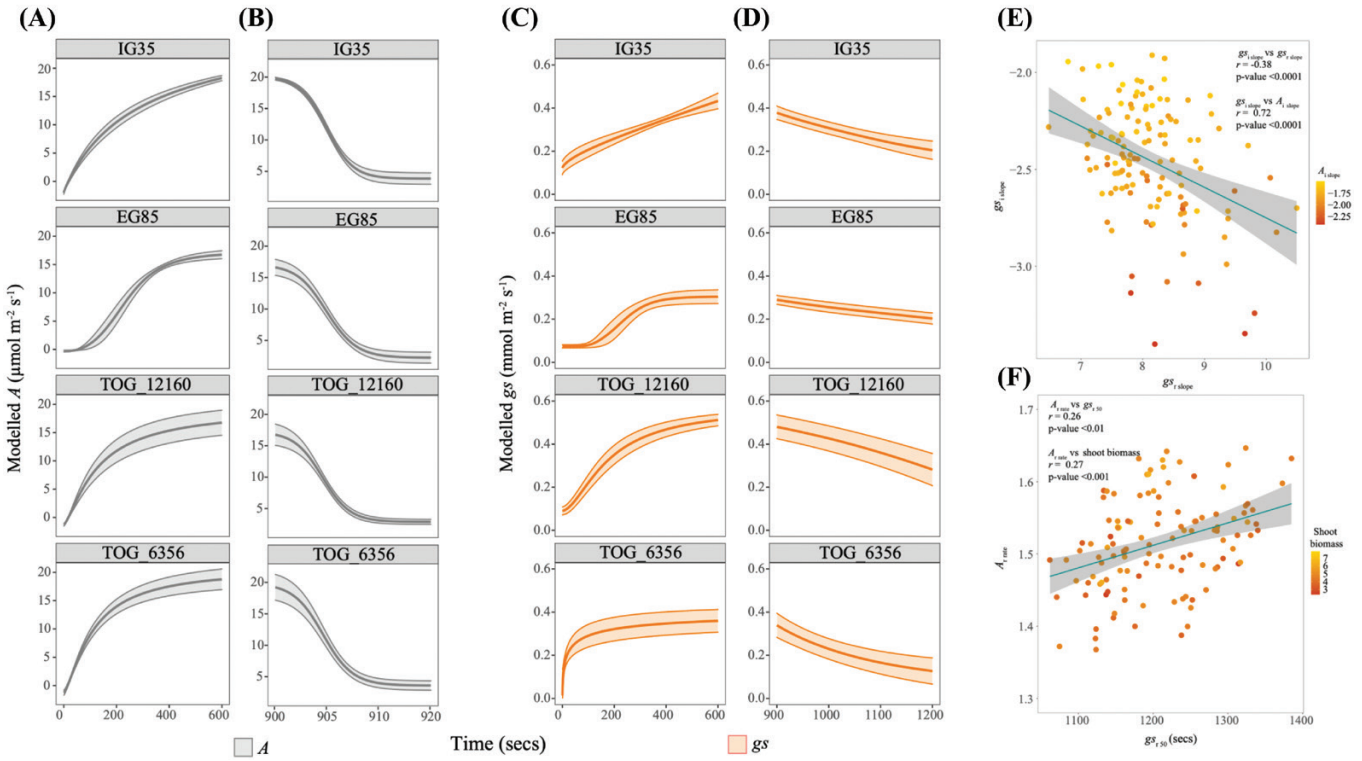

Fig. 5. Demonstrating the variation of (A, B) *A* and (C, D) g_s dynamic responses to light intensity changes within the *O. glaberrima* population using four example accessions. IG35 and TOG_6356 were used as example of a 'slow' and 'fast' responding accession, respectively, whereas EG85 and TOG_12160 are used to demonstrate the intermediate gradient of responses in the population. (E) $g_{si\ slope}$ was correlated with $g_{sr\ slope}$ and $A_{i\ slope}$; during induction, with a greater negative value indicating a steeper slope; this relationship is reversed for the decrease. (F) $A_{r\ rate}$ shows positive associations with $g_{sr\ 50}$ and shoot biomass.

limit ($NPQ_{i\ max}$ and $NPQ_{r\ max}$) was close to the measured value for NPQ_{max}, providing confidence in the method (Table 1; Supplementary Fig. S5C)

We observed limited significance between the kinetics of NPQ relaxation and kinetics of *A*. Importantly, there was a significant negative correlation between the *A* reduction curve lower limit ($A_{r\ min}$) achieved under 100 PPFD, and $NPQ_{r\ slope}$, $NPQ_{r\ 50}$, and $NPQ_{r\ 90}$, suggesting that *A* maintains a higher value under low light conditions when NPQ relaxes rapidly (Kromdijk *et al.*, 2016). Additionally $NPQ_{i\ slope}$, $NPQ_{i\ rate}$, and the time taken to induce 90% of the maximum ($NPQ_{i\ 90}$) strongly correlated with A_{max}.

Speed of induction was not closely related to NPQ capacity: only the time taken to reach 90% of the NPQ curve upper limit ($NPQ_{i\ 90}$) positively correlated to a greater NPQ_{max}. Like gas exchange traits, NPQ induction and relaxation traits were positively correlated ($NPQ_{i\ slope}$ versus $NPQ_{r\ slope}$ and $NPQ_{i\ rate}$ versus $NPQ_{r\ rate}$).

Interestingly, NPQ and g_s dynamic traits also showed numerous significant correlations. $g_{si\ slope}$ significantly correlated with $NPQ_{i\ slope}$, $NPQ_{i\ 10}$, $NPQ_{i\ 50}$, and $NPQ_{i\ 90}$. $g_{si\ rate}$ was positively related to $NPQ_{i\ slope}$ and $NPQ_{i\ 90}$. Accessions with steeper $g_{sr\ slope}$ were also found to have a greater $NPQ_{r\ rate}$ (Fig. 6D). These associations highlight a complex interdependent relationship between g_s, *A*, and NPQ and the recent link noted between underlying control of NPQ by PsbS and the dynamics of stomatal conductance and gas exchange (Fig. 6C, D) (Kromdjik *et al.*, 2016; Glowacka *et al.*, 2018).

Further NPQ relaxation traits were related to morphological and SD traits, indicating that photoprotection has a role in determining growth. $NPQ_{i\ slope}$ and $NPQ_{i\ 90}$ (Fig. 6E) showed negative correlations with shoot biomass and shoot area. $NPQ_{i\ rate}$ positively correlated to shoot biomass and shoot area. A more pronounced set of associations was observed during NPQ relaxation; shoot biomass and shoot area, respectively, showed negative correlations to $NPQ_{r\ slope}$, $NPQ_{r\ 50}$, and $NPQ_{r\ 90}$ (Fig. 6F), and positive correlations to $NPQ_{r\ 10}$ and $NPQ_{r\ rate}$. Root biomass showed a similar, but not as strong, association with $NPQ_{r\ slope}$, $NPQ_{r\ 10}$, $NPQ_{r\ 90}$, and $NPQ_{r\ rate}$.

Trait and ecological comparison between O. glaberrima *and* O. sativa

It is informative to compare the *O. glaberrima* trait variation with that of the elite Asian *O. sativa* cultivar, IR64 (File S3 at Zenodo; Table 1) even though caution should be observed using just one genotype. We highlight the slower induction rates of photosynthesis of IR64.

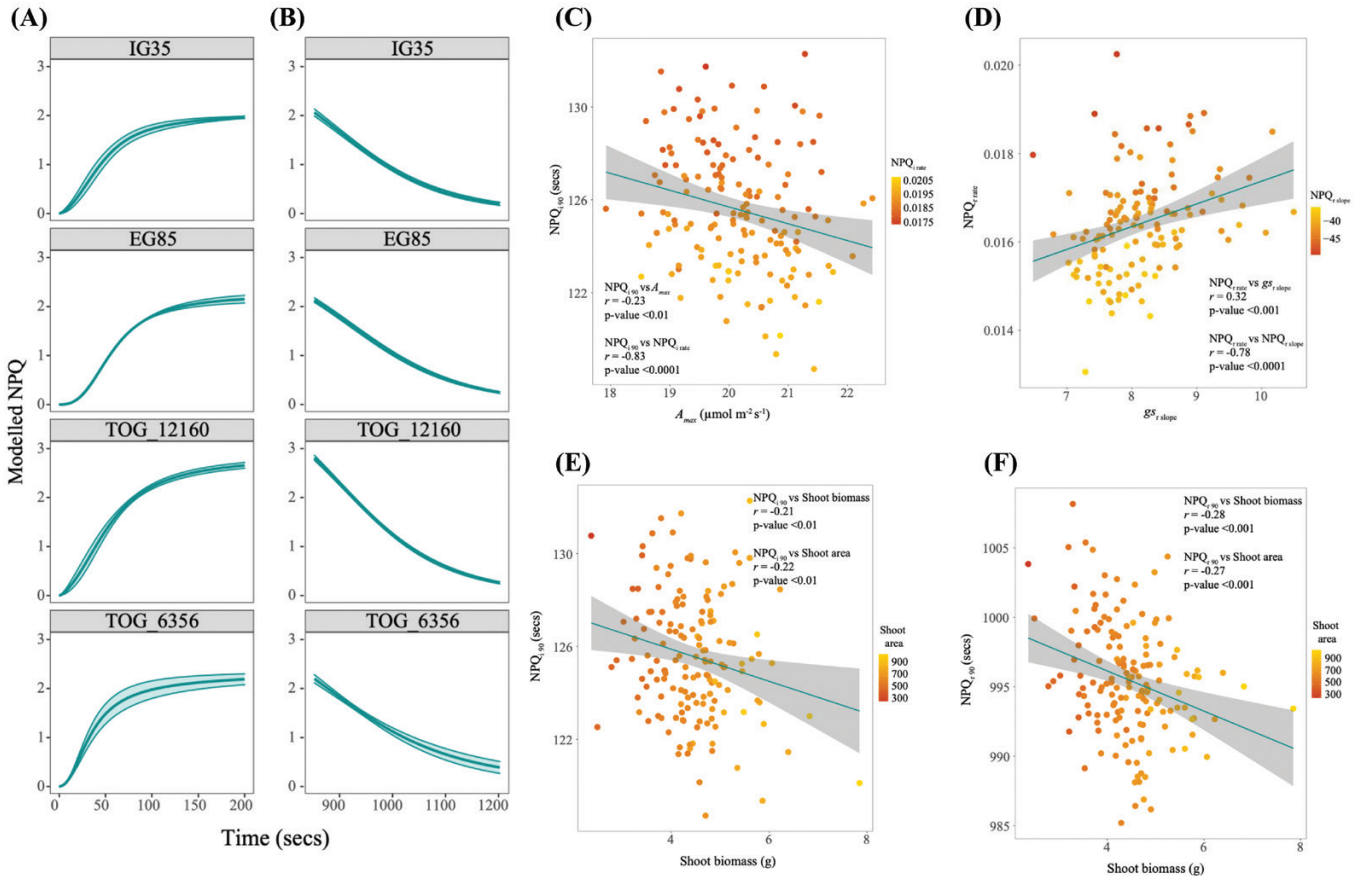

Fig. 6. Demonstrating the variation of NPQ (A) induction and (B) relaxation responses to light intensity changes within the *O. glaberrima* population using four example accessions, as explained in Fig. 5. (C) Negative correlations were identified with $NPQ_{i\ 90}$ against A_{max} and $NPQ_{i\ rate}$. (D) $NPQ_{r\ rate}$ showed a positive relationship to $g_{sr\ slope}$, where a high value indicates a steeper slope and a negative correlation between $NPQ_{r\ rate}$ and $NPQ_{r\ slope}$, where for this model a more negative value suggests a steeper relaxation slope. $NPQ_{i\ 90}$ (E) and $NPQ_{r\ 90}$ (F) showed associations with both shoot biomass and shoot area.

IR64 had a slightly smaller shoot than *O. glaberrima* but a greater root biomass, reflected in the lower shoot:root ratio of IR64, suggesting a greater investment in roots. IR64 height was lower. IR64 displayed a greater SD on the abaxial leaf side than *O. glaberrima*, and IR64 had a lower SD ratio.

IR64 did not differ from *O. glaberrima* for A_{max} and NPQ_{max}. However, average ETR_{max} and $\phi PSII_{max}$ were higher in IR64. IR64 showed a slightly lower g_{smax} and greater $iWUE_{max}$ in comparison with *O. glaberrima*. The latter is likely to be a direct result of the higher levels of g_{smax} observed in *O. glaberrima*. Clear differences were found in dynamics of A, g_s, and NPQ between the two species.

During induction, IR64 was significantly slower than *O. glaberrima* for $g_{si\ 10}$, $g_{si\ 50}$, $A_{i\ 10}$, $A_{i\ 50}$, $A_{i\ 90}$, $A_{i\ rate}$, $NPQ_{i\ 10}$, and $NPQ_{i\ 50}$ (Supplementary Fig. S4). This implies that IR64 had a longer g_s and NPQ lag phase. The initial rapidity of the g_s induction curve may facilitate the significantly faster A response observed in *O. glaberrima*, suggesting that *O. glaberrima* may be able to respond better to the onset of high light than IR64. During the decrease, IR64 and *O. glaberrima* did not significantly differ for $g_{sr\ 10}$, $g_{sr\ 50}$, $g_{sr\ 90}$, $g_{sr\ rate}$, $A_{r\ 10}$, $A_{r\ 90}$, $A_{r\ rate}$, $NPQ_{r\ 10}$, and $NPQ_{r\ rate}$. IR64 was found to have a faster reduction response for $A_{r\ 50}$, $NPQ_{r\ 50}$, and $NPQ_{r\ 90}$ in comparison with *O. glaberrima* (Table 1 in comparison with File S3 at Zenodo).

During the multivariate analyses, we observed that *O. sativa* IR64 values cluster separately from *O. glaberrima* for both ecology and country of origin. This can be seen most clearly when plotting principal components (PCs) 1 and 3, where the two species cluster distinctly for the Asian country of origin and paddy field ecology (Fig. 8C).

Impact of country of origin and ecotype on O. glaberrima *trait adaptation*

An important aspect of *O. glaberrima*'s novelty is the independent evolution to *O. sativa* and adaptation to the variable African environment. We used PCA and H-clustering to explore natural trait variation and the adaptive effect of environmental climatic variables. Here we identify phenotypic trends which cluster according to country and environment, indicating adaptation and possibly variation in growth strategy.

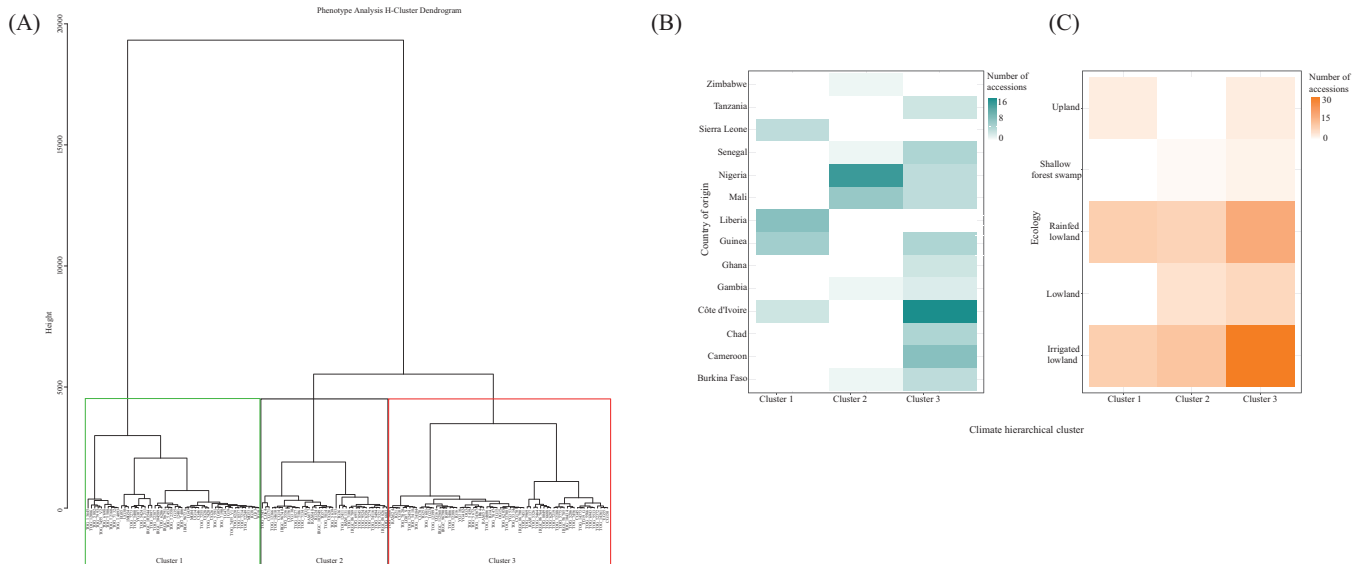

Fig. 7. Hierarchical clustering of 155 *O. glaberrima* accessions (A) for 64 phenotypic traits and the frequency of accessions for each country of origin (B) and ecological niche (C) in the clades (1–3) identified in the climate hierarchical clustering analysis.

The PCA and H-clustering were separated into two grouped analyses for phenotypic and climatic variables. For the PCA of phenotypic traits 12 PCs were selected as they explain 95% of the variance (Supplementary Fig. S6). The H-clustering analysis identified three clusters (Fig. 7A) with common sources of trait variation (File S7 at Zenodo). The accessions in cluster 1 are characterized by a slow g_s reduction time ($g_{sr\ 10/50/90}$), rapid A and NPQ induction time ($A_{i\ 50}$ and $NPQ_{i\ 90}$), steep A reduction curve ($A_{r\ slope}$), rapid A reduction time ($A_{r\ 50/90}$), high values for g_{smax}, $A_{r\ rate}$, $NPQ_{i\ rate}$, and shoot:root ratio, and low values for root biomass, VPD_{max}, and $iWUE_{max}$. Accessions present in cluster 2 demonstrate g_s reduction curves with a steep slope and rapid reduction times ($g_{sr\ 10/50/90}$), high trait values for NPQ_{max}, VPD_{max}, and $iWUE_{max}$, and low values for plant biomass, shoot biomass, shoot area, g_{smax}, ETR_{max}, and $\phi PSII_{max}$. Accessions in the largest group, cluster 3, show high trait values for total biomass, shoot biomass, shoot area, root biomass, and A_{max}, low levels of NPQ ($NPQ_{r\ min}$) under reduced light (100 PPFD), and rapid g_s reduction time ($g_{sr\ 50/90}$). Cluster 3 is the group where IR64 can be found, and it consists mostly of lowland type accessions.

Adaptation to different environments was explored during the multivariate analyses. In Fig. 8A and B, axes PC1 and 2 are shown overlaid with ecological niche and country of origin. *Oryza glaberrima* accessions cluster separately dependent upon their ecological origin, in particular upland or lowland (Fig. 8B). Accessions from lowland-type ecologies dominate, though it is still clear that upland and lowland show trait differences. Accessions also show a high degree of trait variation due to countries of origin that have contrasting climates (Fig. 8A). For example, distinct clustering can be seen between landlocked Burkina-Faso, which borders the Sahara, and coastal Gambia. A categorical analysis was performed to establish if the accessions that occupy each cluster of the H-clustering analysis share similar origins (Supplementary Fig. S7B, C). While there is no obvious relationship, a greater proportion of upland accessions occupy cluster 1, whereas a large proportion of lowland accessions are present in cluster 3 (Supplementary Fig. S7C).

The diversity of climates and elevations (Fig. 2A–C) are likely to have directly impacted trait adaptation and resilience. A PCA focused on climatic traits explored the relationship between climate and phenotype. The first four PCs explain 90% of trait variation in the population (File S8 at Zenodo). H-clustering identified three distinct clusters of accessions with common sources of variation in climatic variables (Files S9, S11 at Zenodo). A categorical analysis of ecological niche and country of origin for the accessions present in each cluster showed a clear distinction of climate-based clustering due to country of origin (Fig. 7C). Cluster 1 contains all accessions that originate from the neighbouring countries of Liberia and Sierra Leone. Cluster 2 contains all accessions from Zimbabwe and most accessions originating from Nigeria. Cluster 3, which contains the largest number of accessions, contains all individuals originating from Cameroon, Chad, Ghana, and Tanzania, and the majority of accessions from Côte d'Ivoire and Senegal.

With the extensive phenotypic and climatic variables reduced to a small number of components, we completed a correlation analysis between the phenotypic and climatic trait PCs to identify groups of climatic drivers on trait adaptation. A significant positive association was identified between trait PC1 and climatic PC4 (r= –0.20, P<0.05; Fig. 8D), suggesting that key traits contributing to phenotypic trait PC1, which includes photosynthetic traits and shoot biomass, have adapted in response to precipitation-related variables that contribute to climate PC4 loadings. Other significant associations were identified between phenotype PC5 and climate PC4 (r=0.25,

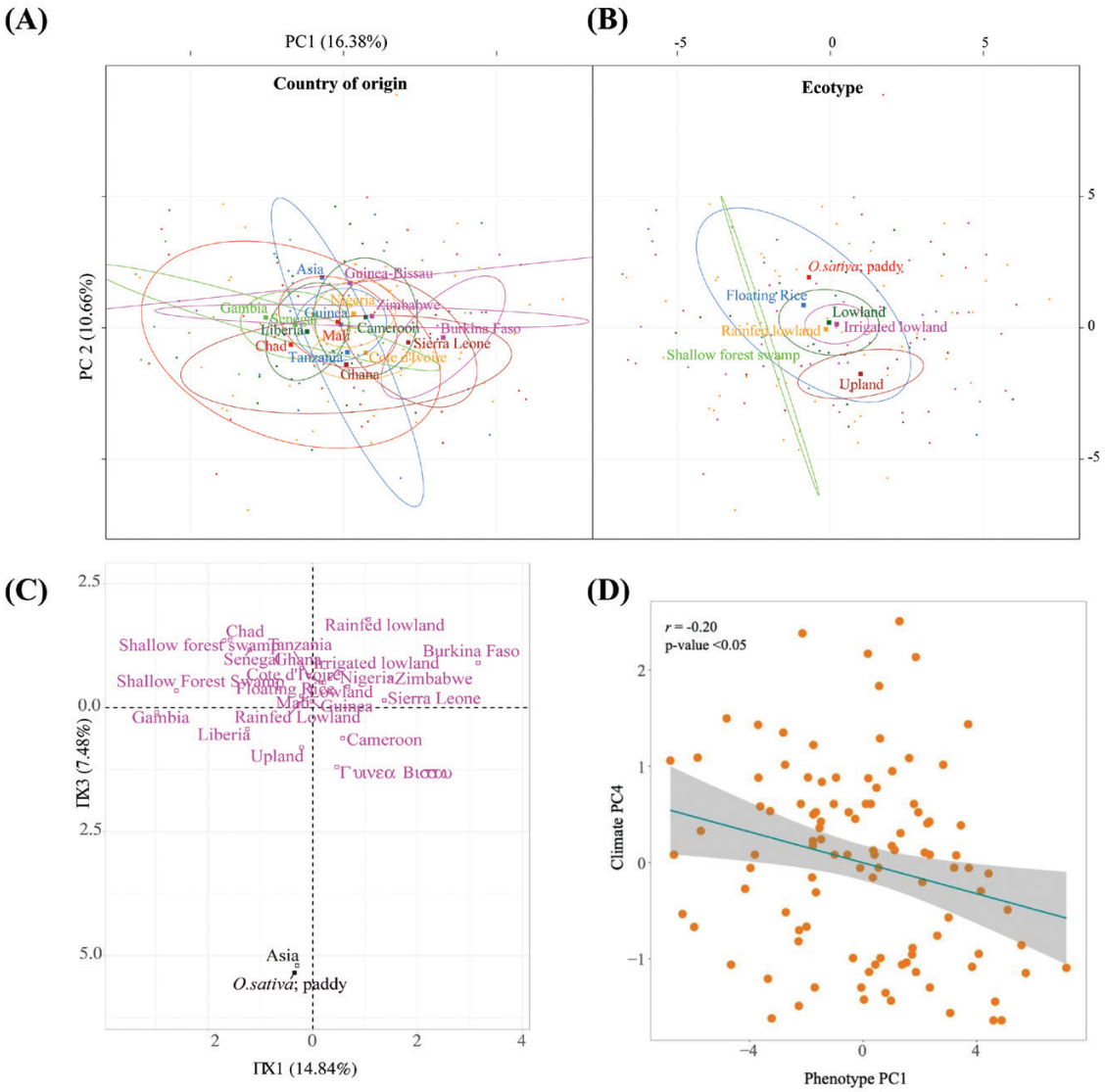

Fig. 8. Graphical PCA outputs; the phenotypic PCs 1 and 2 are overlaid with 95% confidence ellipses for the *O. glaberrima* accessions; (A) country of origin and (B) ecotype categorical variables. (C) PCs and 3 show the separate clustering of *O. sativa* (IR64), based on country of origin and ecotype categories, from *O. glaberrima*. (D) PC1 from the phenotypic traits data PCA was found to be a function of PC4 from the climatic data PCA analysis.

$P<0.05$), phenotype PC8 and climate PC2 ($r=0.24$, $P<0.05$), and phenotype PC11 and climate PC3 ($r=0.25$, $P<0.05$) File S12; Supplementary Fig. S8).

Discussion

Crop production in future climates has the challenge of increasing productivity whilst retaining resilience. To do so, optimizing interactions and trade-offs between carbon assimilation, photoprotection, and water loss will be essential. However, we do not yet have complete understanding of the genetic basis of the co-regulation of the interlinked processes and components (light harvesting, photoprotection, electron transport, carbon assimilation, and stomatal conductance) involved. Recent progress shows that crop productivity and WUE are only partly dependent upon 'steady-state' maximum values of A_{max} and g_{smax}. SD, stomatal conductance, and photoprotection dynamics have been identified as critical traits to optimize carbon assimilation and minimize abiotic stress (Kromdijk *et al.*, 2016; Caine *et al.*, 2019; Faralli *et al.*, 2019). However, elite gene pools may be genetically narrow and poorly adapted to challenging environmental conditions. Attention is increasingly focused upon underutilized crop species and wild relatives as a source of genetic diversity to improve resilience in commercial species (Draic *et al.*, 2011). Whilst the variation for photosynthesis induction has been partly characterized in *O. sativa*, this is not true of *O. glaberrima* (Acevedo-Siaca *et al.*, 2020, 2021). The *O. glaberrima* association panel used here was developed as a resource for crop improvement, which may have diversity not

available in *O. sativa* (Agnoun *et al.*, 2012). For the first time, a comprehensive analysis of photosynthesis- and morphology-related traits has been completed in *O. glaberrima*. Our novel approach uses a large pool of accessions, with a large range of heritable natural variation to explore the natural variation and relationships in these traits. While we cannot here make a meaningful comparison between *O. glaberrima* and *O. sativa*, we observed key differences, with the former showing faster photosynthesis induction. This may be an indication of adaptation to drier soils and air generally, requiring faster opening and closure of stomata (Lawson and Vialet-Chabrand, 2019).

Here we have described extensive natural variation in *O. glaberrima* for steady-state, induction, and relaxation/reduction responses for A and g_s. This suggests underlying genetic diversity to these traits that could be identified and exploited. We identified indications of heritability (H^2) and underlying genetic variation (PGV) in many of these traits (Table 1). Trait heritability values were comparable with estimates of similar traits from maize (Choquette *et al.*, 2019), but they are marginally lower than those previously demonstrated in *O. sativa* (Qu *et al.*, 2017), though a strong genetic component is still indicated. A calculation of heritability using genomic data would provide a more accurate estimation (Zhu and Zhou, 2020). This would be useful when selecting traits for genetic introgression or characterization. The large number of accessions used here (155) permits a statistical comparison that was not possible in related studies on dynamic photosynthesis in *O. sativa* where fewer lines were analysed (Acevedo-Siaca *et al.*, 2020).

A global PCA and clustering analysis showed a distinction between clusters of high biomass (cluster 3), low biomass (cluster 2), and low root biomass (cluster 1). The fast g_s decrease, low g_{smax}, high NPQ_{max}, and high $iWUE_{max}$ of cluster 2 would suggest a conservative type geared toward water conservation, whilst the high total biomass of cluster 3 is consistent with a fast growth type displaying a rapid g_s decrease, low NPQ, and a higher A_{max}. The association of cluster 3 with wetter lowland environments is consistent with higher productivity. We therefore see a general consistency in these two clusters with photosynthetic, water use, and biomass production 'strategy'. It is also notable that steady-state A_{max} correlates well with biomass, suggesting that capacity for higher photosynthesis is still important. Increases in photosynthetic capacity are known to improve light responses in rice (Sun *et al.*, 2016).

Extensive natural variation identified in dynamic photosynthetic traits

In recent years, there has been a shift in photosynthesis-related research towards dynamic responses in place of steady-state values. It is now recognized that irradiance fluctuations in field conditions, and the ability of stomatal and photosynthetic responses to respond instantaneously, can substantially affect plant productivity (Taylor and Long, 2017). To enable greater productivity in dynamic environments such as a crop canopy, one would anticipate that all components of photosynthesis would respond rapidly to 'track' light closely. Each component has a different effect; thus, fast activation of the Calvin cycle and CO_2 assimilation during induction is beneficial, while rapid reduction of NPQ and fast stomatal closure at transition to low light enable the attainment of improved CO_2 efficiency and iWUE at low light.

It is clear that we see some independence of dynamic traits, but interesting associations appear which indicate a link with biomass. Recent research suggests that major yield gains can be made by enhancing photoprotection capacity and NPQ dynamic responses (Kromdijk *et al.*, 2016; Hubbart *et al.*, 2018). Rapid NPQ relaxation can remove the limitation on quantum yield of CO_2 assimilation, allowing a quicker recovery of photosynthetic efficiency upon A reduction (Kromdijk *et al.*, 2016; Murchie and Ruban, 2020). Our findings support this: NPQ relaxation dynamics were the only group found to have ubiquitous associations with increased shoot biomass and area. Notably, we also observed that values for A under low light were greater in those accessions that exhibited rapid NPQ relaxation and those that have lower NPQ capacity under low light ($NPQ_{r\ min}$). It is also hypothesized that faster induction of CO_2 assimilation may reduce the need for photoprotection during induction (McAusland and Murchie, 2020); however, we found no association between A induction traits and NPQ dynamic or steady-state values. We did find that faster NPQ induction is associated with greater photosynthetic capacity, shoot area, and biomass.

Whilst no associations were identified between NPQ and A reduction dynamics, we found strong positive correlations between the speed of g_s and NPQ dynamics. This may highlight the importance of the key NPQ protein, PSII subunit S (PsbS), on stomatal conductance, as shown by Głowacka *et al.* (2018), whereby PsbS overexpression, which increases both NPQ capacity and NPQ dynamic rate (Kromdijk *et al.*, 2016; Głowacka *et al.*, 2018; Hubbart *et al.*, 2018), also reduces the extent of stomatal opening in tobacco. This may be reflected here by the negative correlation between NPQ_{max} and g_{smax}, also that the g_s induction rate was lower when NPQ induction was faster. This highlights the need to further explore the associations between NPQ and g_s dynamics: these have not been elucidated although there is a general principle that limitations imposed by g_s or Rubisco activation state would result in a further reduction of electron transport and an enhanced NPQ. We suggest that in *O. glaberrima* NPQ may be a major player in both g_s and A reduction dynamics. Akin to the relationship between A and g_s, there is a trade-off in NPQ as it reduces photosynthetic quantum yields under low irradiance.

No association was identified between the water use-related traits, g_s and $iWUE_{max}$, and SD; this may be because the variation was less than that needed to produce changes in gas exchange traits (Caine *et al.*, 2019; Mohammed *et al.*, 2019). It is also possible that this highlights the importance of stomatal size

and morphology, rather than density, on these traits. Smaller stomata have been shown to have improved WUE, g_{smax}, and dynamics (Drake *et al.*, 2013; Dittberner *et al.*, 2018; Lawson and Vialet-Chabrand, 2019; Chatterjee *et al.*, 2020). However, the positive correlations we identified between SD ratio, NPQ_{max}, and the level of NPQ achieved under low light ($NPQ_{r\ min}$) is unusual. The significant negative association between SD ratio and $A_{r\ rate}$ has no direct interpretation but may indicate that the SD ratio is a trait worthy of further work. Upper leaf SD had positive relationships to $g_{si\ 50}$ and $A_{r\ rate}$, and negative to $g_{sr\ min}$, also indicating that distinction between the leaf surfaces may be important.

Understanding the interplay of photoprotective, stomatal, and assimilation dynamics should include detailed morphological characterization (Ohsumi *et al.*, 2007; Drake *et al.*, 2013; McAusland *et al.*, 2016), together with the associated mesophyll conductance (Campany *et al.*, 2016; Deans *et al.*, 2019). The proportion by which photosynthetic dynamics are limited by stomata or biochemistry seems to be species dependent (Tinoco-Ojanguren and Pearcy, 1993; Taylor and Long, 2017; De Souza *et al.*, 2020). *Oryza sativa* photosynthetic induction has been shown to be predominantly limited by biochemistry (Acevedo-Siaca *et al.*, 2020, 2021), and the same assumption might be extended to *O. glaberrima* due to a similar genomic composition (Stein *et al.*, 2018); however, we conclude from our data that stomatal limitations may be more pronounced in *O. glaberrima*.

Accessions have adapted to variable ecological and environmental regimes in different countries

No comprehensive studies exist that tease apart the ecological and environmental variables that correlate with specific trait adaptation in *O. glaberrima*. This information is useful from an evolutionary perspective but may be essential in the selection of cultivars for abiotic stress tolerance varieties and trait-related genetic characterization.

Of note, we identified a significant association between the climate PC4 and phenotype PC1 (Fig. 8D; File S12 at Zenodo). This relationship suggests that key photosynthetic traits contributing to PC1 have adapted in response from climatic pressures associated with PC4, such as elevation and the combined effect of temperature and precipitation. However, these are broad observations for climatic–trait correlations across the African continent, lacking resolution that can be seen in studies on a discrete geographical area (Wolfe and Tonsor, 2014).

For the selection of abiotic stress tolerance-adapted cultivars, the H-clustering analyses would be of particular use, as this generated three distinct clades of *O. glaberrima* accessions stemming from similar climatic and phenotypic variables. Furthermore, the climatic H-clustering demonstrated clear grouping of accessions due to country of origin (Fig. 7B), suggesting that a higher resolution analysis of environmental effect on trait adaptation would be beneficial.

We identified adaptation based upon ecotype in the PCA (Fig. 8B), supporting a known distinction between *O. glaberrima* upland and lowland phenotypes (Ghesquière, 1997). However, there is no comprehensive description in the literature of the physiological differences that contribute to these ecotypes. Though due to the unequal representation of accessions from each ecological niche in this analysis, it is difficult to obtain a clear indication of the effect of ecotype on trait adaptation.

The environmental analysis completed here produces useful information of accessions displaying similar phenotypic qualities because of environmental adaptation. Equally, this also highlights the requirement for a dedicated study to truly elucidate the environmental and ecological trait adaptation of *O. glaberrima*, utilizing equally represented accessions from a range of ecotypes and assessing physiological adaptation to climatic variables at a range of spatial scales.

Conclusions

Here, we have demonstrated that *O. glaberrima* has broad, heritable natural variation in a range of important traits, which are likely to aid in the improvement of *O. sativa*. This is the first study to describe photosynthetic, photoprotection, and dynamic traits in *O. glaberrima*, the size of which is not matched in panels of *O. sativa* accessions. The phenotyping efforts compiled here will provide a basis for the identification of interesting traits for physiology research, aid in the selection of accessions for crop improvement efforts, and provide information for genetic characterization.

Supplementary data

The following supplementary data are available at *JXB* online.

Fig. S1. Original, un-fitted data for induction and reduction of CO_2 assimilation (A), stomatal conductance (gs) and NPQ vs time.

Fig. S2. Correlations between the best linear unbiased predictor (BLUP) values and the original mean.

Fig. S3. Correlation matrix of all phenotypic traits measured.

Fig. S4. Modelled curves for two extreme *O. glaberrima* accessions and *O. sativa* IR64, plotted on a log scale.

Fig. S5. Linear regression plots showing strong positive correlations between the actual measurement vs modelled estimate values.

Fig. S6. Plots showing the scree plot and trait loadings for the phenotypic data PCA analysis.

Fig. S7. H-clustering dendrogram of 105 *O. glaberrima* accessions and frequency plots generated from the H-clustering analysis of the phenotypic data from 155 *O. glaberrima* accessions.

Fig. S8. Correlation matrix for all phenotypic and climatic data, alongside their principal components.

Table S1. List of parameter abbreviations, definitions and units of measurement.

Table S2. List of *O. glaberrima* ID codes, country of origin and ecology.

Table S3. Estimated model outputs.

Acknowledgements

We would like to acknowledge the life and scientific rigour of Dr Pracha Treeingtong. Pracha sadly passed away upon the commencement of this manuscript. Our heartfelt condolences and thoughts are with Pracha's friends and family. We would like to thank Dr François Sabot and Dr Philippe Cubry from RICE, CIRAD, Montpelier for their hard work in the development of this *O. glaberrima* germplasm as a resource. We would also like to thank Dr Marie-Noelle Ndjiondjop from AfricaRice for providing us with the ecological information for each *O. glaberrima* accession and her ongoing dedication to its research. We would also like to thank the software developer, Matthew Hartley, who wrote the Python code 'DataProcessor' and helped to develop loops in R-Studio to manage the large volume of data produced in this study.

Author contributions

EHM, SM, and RS: conceptualization; SBC with input from PT: investigation, data curation, formal analysis; SBC with input from JF, HS, and PT: methodology; SBC with input from EHM: writing—original draft; RS, SM, and EHM: funding acquisition; SBC, EHM, SM with input from JF, RS: writing—review and editing; SM, EHM, and RS: project administration.

Conflict of interest

The authors declare no conflicts of interest.

Funding

SC is in receipt of a BBSRC PhD scholarship as part of the Nottingham Doctoral Training Partnership. EM receives funding from the Biotechnology and Biological Sciences Research Council [grant no. BB/R004633/1].

Data availability

Data supporting the findings of this study are available within the paper and within its supplementary data published online. The data Files (S1–S12) are deposited at the Zenodo repository: https://doi.org/10.5281/zenodo.5555930; Murchie, 2021. Any other data are available from the corresponding author upon request.

References

Acevedo-Siaca LG, Coe R, Quick WP, Long SP. 2021. Variation between rice accessions in photosynthetic induction in flag leaves and underlying mechanisms. Journal of Experimental Botany **72**, 1282–1294.

Acevedo-Siaca LG, Coe R, Wang Y, Kromdijk J, Quick WP, Long SP. 2020. Variation in photosynthetic induction between rice accessions and its potential for improving productivity. New Phytologist **227**, 1097–1108.

Agnoun Y, Biaou SSH, Sié M, Vodouhè RS, Ahanchédé A. 2012. The African rice *Oryza glaberrima* Steud: knowledge distribution and prospects. International Journal of Biology **4**, 158.

Atwell BJ, Wang H, Scafaro AP. 2014. Could abiotic stress tolerance in wild relatives of rice be used to improve *Oryza sativa*? Plant Science **215–216**, 48–58.

Barratt GE, Sparkes DL, Mcausland L, Murchie EH. 2021. Anisohydric sugar beet rapidly responds to light to optimize leaf water use efficiency utilizing numerous small stomata. AoB Plants **13**, doi: 10.1093/aobpla/plaa067

Bimpong IK, Serraj R, Chin JH, *et al.* 2011. Identification of QTLs for drought-related traits in alien introgression lines derived from crosses of rice (*Oryza sativa* cv. IR64) × *O. glaberrima* under lowland moisture stress. Journal of Plant Biology **54**, 237–250.

Black R, Allen L, Bhutta Z. 2008. Climate change, food insecurity and hunger: key messages for UNFCCC negotiators. http://www.careclimatechange.org/files/reports/IASC_CC_FS.pdf

Blum A. 2009. Effective use of water (EUW) and not water-use efficiency (WUE) is the target of crop yield improvement under drought stress. Field Crops Research **112**, 119–123.

Bocco R, Lorieux M, Seck PA, Futakuchi K, Manneh B, Baimey H, Ndjiondjop MN. 2012. Agro-morphological characterization of a population of introgression lines derived from crosses between IR 64 (*Oryza sativa indica*) and TOG 5681 (*Oryza glaberrima*) for drought tolerance. Plant Science **183**, 65–76.

Burgess AJ, Retkute R, Preston SP, Jensen OE, Pound MP, Pridmore TP, Murchie EH. 2016. The 4-dimensional plant: effects of wind-induced canopy movement on light fluctuations and photosynthesis. Frontiers in Plant Science **7**, 1392.

Caine RS, Yin X, Sloan J, *et al.* 2019. Rice with reduced stomatal density conserves water and has improved drought tolerance under future climate conditions. New Phytologist **221**, 371–384.

Campany CE, Tjoelker MG, von Caemmerer S, Duursma RA. 2016. Coupled response of stomatal and mesophyll conductance to light enhances photosynthesis of shade leaves under sunflecks. Plant, Cell & Environment **39**, 2762–2773.

Challinor AJ, Watson J, Lobell DB, Howden SM, Smith DR, Chhetri N. 2014. A meta-analysis of crop yield under climate change and adaptation. Nature Climate Change **4**, 287–291.

Chatterjee J, Thakur V, Nepomuceno R, *et al.* 2020. Natural diversity in stomatal features of cultivated and wild *Oryza* species. Rice **13**, 58.

Choquette NE, Ogut F, Wertin TM, Montes CM, Sorgini CA, Morse AM, Brown PJ, Leakey ADB, McIntyre LM, Ainsworth EA. 2019. Uncovering hidden genetic variation in photosynthesis of field-grown maize under ozone pollution. Global Change Biology **25**, 4327–4338.

Cubry P, Pidon H, Ta KN, *et al.* 2020. Genome wide association study pinpoints key agronomic QTLs in African rice *Oryza glaberrima*. Rice **13**, 66.

Deans RM, Brodribb TJ, Busch FA, Farquhar GD. 2019. Plant water-use strategy mediates stomatal effects on the light induction of photosynthesis. New Phytologist **222**, 382–395.

De Souza AP, Wang Y, Orr DJ, Carmo-Silva E, Long SP. 2020. Photosynthesis across African cassava germplasm is limited by Rubisco and mesophyll conductance at steady state, but by stomatal conductance in fluctuating light. New Phytologist **225**, 2498–2512.

Dittberner H, Korte A, Mettler-Altmann T, Weber APM, Monroe G, de Meaux J. 2018. Natural variation in stomata size contributes to the local adaptation of water-use efficiency in *Arabidopsis thaliana*. Molecular Ecology **27**, 4052–4065.

Draic P, Flood J, Harbinson J, Aarts MGM. 2011. Natural genetic variation in plant photosynthesis. Trends in Plant Science **16**, 327–335.

Drake PL, Froend RH, Franks PJ. 2013. Smaller, faster stomata: scaling of stomatal size, rate of response, and stomatal conductance. Journal of Experimental Botany **64**, 495–505.

Faralli M, Matthews J, Lawson T. 2019. Exploiting natural variation and genetic manipulation of stomatal conductance for crop improvement. Current Opinion in Plant Biology **49**, 1–7.

Ghesquière A, Séquier J, Second G, Lorieux M. 1997. First steps towards a rational use of African rice, *Oryza glaberrima*, in rice breeding through a 'contig line' concept. Euphytica **96**, 31–39.

Głowacka K, Kromdijk J, Kucera K, Xie J, Cavanagh AP, Leonelli L, Leakey ADB, Ort DR, Niyogi KK, Long SP. 2018. Photosystem II Subunit S overexpression increases the efficiency of water use in a field-grown crop. Nature Communications **9**, 868.

Gu J, Yin X, Stomph T-J, Struik PC. 2014. Can exploiting natural genetic variation in leaf photosynthesis contribute to increasing rice productivity? A simulation analysis. Plant, Cell & Environment **37**, 22–34.

Hijmans RJ, Cameron SE, Parra JL, Jones PG, Jarvis A. 2005. Very high resolution interpolated climate surfaces for global land areas. International Journal of Climatology **25**, 1965–1978.

Hubbart S, Smillie IRA, Heatley M, Swarup R, Foo CC, Zhao L, Murchie EH. 2018. Enhanced thylakoid photoprotection can increase yield and canopy radiation use efficiency in rice. Communications Biology **1**, 22.

Kromdijk J, Głowacka K, Leonelli L, Gabilly ST, Iwai M, Niyogi KK, Long SP. 2016. Improving photosynthesis and crop productivity by accelerating recovery from photoprotection. Science **354**, 857–861.

Lawson T, Blatt MR. 2014. Stomatal size, speed, and responsiveness impact on photosynthesis and water use efficiency. Plant Physiology **164**, 1556–1570.

Lawson T, Vialet-Chabrand S. 2019. Speedy stomata, photosynthesis and plant water use efficiency. New Phytologist **221**, 93–98.

Lawson T, von Caemmerer S, Baroli I. 2010. Photosynthesis and stomatal behaviour. In: Lüttge U, Beyschlag W, Büdel B, Francis D, eds. Photosynthesis and stomatal behaviour. Progress in Botany 72. Berlin Heidelberg: Springer, 265–304.

Lê S, Josse J, Husson F. 2008. FactoMineR: an R package for multivariate analysis. Journal of Statistical Software **25**, 1–18.

Lin TY, Maire M, Belongie S, Hays J, Perona P, Ramanan D, Dollár P, Zitnick CL. 2014. Microsoft coco: common objects in context. In: Fleet D, Pajdla T, Schiele B, Tuytelaars T, eds. Computer Vision—ECCV 2014. Lecture Notes in Computer Science, vol 8693. Cham: Springer, 740–755.

Linares OF. 2002. African rice (*Oryza glaberrima*): history and future potential. Proceedings of the National Academy of Sciences, USA **99**, 16360–16365.

McAusland L, Murchie EH. 2020. Start me up; harnessing natural variation in photosynthetic induction to improve crop yields. New Phytologist **227**, 989–991.

McAusland L, Vialet-Chabrand S, Davey P, Baker NR, Brendel O, Lawson T. 2016. Effects of kinetics of light-induced stomatal responses on photosynthesis and water-use efficiency. New Phytologist **211**, 1209–1220.

Merk HL, Yarnes SC, Van Deynze A, *et al*. 2012. Trait diversity and potential for selection indices based on variation among regionally adapted processing tomato germplasm. Journal of the American Society for Horticultural Science **137**, 427–437.

Mohammed U, Caine RS, Atkinson JA, Harrison EL, Wells D, Chater CC, Gray JE, Swarup R, Murchie EH. 2019. Author Correction: rice plants overexpressing OsEPF1 show reduced stomatal density and increased root cortical aerenchyma formation. Scientific Reports **9**, 14827.

Murchie EH. 2021. Data from: Natural variation in photosynthetic traits in a diverse population of *Oryza glaberrima*. [Dataset]. Zenodo. Doi: 10.5281/zenodo.5555931

Murchie EH, Kefauver S, Araus JL, Muller O, Rascher U, Flood PJ, Lawson T. 2018. Measuring the dynamic photosynthome. Annals of Botany **122**, 207–220.

Murchie EH, Lawson T. 2013. Chlorophyll fluorescence analysis: a guide to good practice and understanding some new applications. Journal of Experimental Botany **64**, 3983–3998.

Murchie EH, Ruban AV. 2020. Dynamic non-photochemical quenching in plants: from molecular mechanism to productivity. The Plant Journal **101**, 885–896.

Ohsumi A, Kanemura T, Homma K, Horie T, Shiraiwa T. 2007. Genotypic variation of stomatal conductance in relation to stomatal density and length in rice (*Oryza sativa* L.). Plant Production Science **10**, 322–328.

Qu M, Zheng G, Hamdani S, Essemine J, Song Q, Wang H, Chu C, Sirault X, Zhu XG. 2017. Leaf photosynthetic parameters related to biomass accumulation in a global rice diversity survey. Plant Physiology **175**, 248–258.

Ray DK, West PC, Clark M, Gerber JS, Prishchepov AV, Chatterjee S. 2019. Climate change has likely already affected global food production. PLoS One **14**, e0217148.

Ren S, He K, Girshick R, Sun J. 2015. Faster r-cnn: towards real-time object detection with region proposal networks. Advances in Neural Information Processing Systems **39**, 1137–1149.

Ritz C, Baty F, Streibig JC, Gerhard D. 2015. Dose–response analysis using R. PLoS One **10**, e0146021.

Robinson GK. 1991. That BLUP is a good thing: the estimation of random effects. Statistical Science **6**, 15–32.

Sarla N, Swamy BPM. 2005. *Oryza glaberrima*: a source for the improvement of *Oryza sativa*. Current Science **89**, 955–963.

Slattery RA, Walker BJ, Weber APM, Ort DR. 2018. The impacts of fluctuating light on crop performance. Plant Physiology **176**, 990–1003.

Stein JC, Yu Y, Copetti D, *et al*. 2018. Genomes of 13 domesticated and wild rice relatives highlight genetic conservation, turnover and innovation across the genus *Oryza*. Nature Genetics **50**, 285–296.

Sun J, Ye M, Peng S, Li Y. 2016. Nitrogen can improve the rapid response of photosynthesis to changing irradiance in rice (*Oryza sativa* L) plants. Scientific Reports **6**, 30315.

Szegedy C, Vanhoucke V, Ioffe S, Shlens J, Wojna Z. 2016. Rethinking the inception architecture for computer vision. In: Proceedings of the IEEE conference on computer vision and pattern recognition. Las Vegas, NV, 2818–2826.

Taylor SH, Long SP. 2017. Slow induction of photosynthesis on shade to sun transitions in wheat may cost at least 21% of productivity. Philosophical Transactions of the Royal Society B: Biological Sciences **372**, 20160543.

Tinoco-Ojanguren C, Pearcy RW. 1993. Stomatal dynamics and its importance to carbon gain in two rainforest Piper species - I. VPD effects on the transient stomatal response to lightflecks. Oecologia **94**, 388–394.

Wambugu PW, Ndjiondjop MN, Henry R. 2019. Advances in molecular genetics and genomics of African rice (*Oryza glaberrima* Steud). Plants **8**, 376.

Wolfe MD, Tonsor SJ. 2014. Adaptation to spring heat and drought in northeastern Spanish *Arabidopsis thaliana*. New Phytologist **201**, 323–334.

York LM. 2018. Phenotyping crop root crowns: general guidance and specific protocols for maize, wheat, and soybean. Methods in Molecular Biology **1761**, 23–32.

Zhao C, Liu B, Piao S, *et al.* 2017. Temperature increase reduces global yields of major crops in four independent estimates. Proceedings of the National Academy of Sciences, USA **114**, 9326–9331.

Zhu H, Zhou X. 2020. Statistical methods for SNP heritability estimation and partition: a review. Computational and Structural Biotechnology Journal **18**, 1557–1568.